energies

MDPI

Article

Controls of Radiogenic Heat and Moho Geometry on the Thermal Setting of the Marche Region (Central Italy): An Analytical 3D Geothermal Model

Stefano Santini [1], Matteo Basilici [2], Chiara Invernizzi [2], Danica Jablonska [2], Stefano Mazzoli [2], Antonella Megna [3,*] and Pietro Paolo Pierantoni [2]

1 Dipartimento di Scienze Pure e Applicate (DiSPeA), Università di Urbino "Carlo Bo", Via Aurelio Saffi, 2, 61029 Urbino, Italy; stefano.santini@uniurb.it
2 Scuola di Scienze e Tecnologie, Sezione di Geologia, Università degli Studi di Camerino, Via Gentile III da Varano, 7, 62032 Camerino, Italy; matteo.basilici@unicam.it (M.B.); chiara.invernizzi@unicam.it (C.I.); danica.jablonska@unicam.it (D.J.); stefano.mazzoli@unicam.it (S.M.); pietropaolo.pierantoni@unicam.it (P.P.P.)
3 Istituto Nazionale di Geofisica e Vulcanologia (INGV), Sezione di Sismologia e Tettonofisica, 00143 Rome, Italy
* Correspondence: antonella.megna@ingv.it

Abstract: Using published cross-sections and a series of geological constraints, a 3D geological model of an important area of the Adriatic sector of peninsular Italy—i.e., the Marche region—was developed. Then, an analytical procedure, taking into account the heat rising from the mantle and the radiogenic heat produced by the crust, was applied on the pre-built structural model, in order to obtain the 3D geothermal setting of the entire region. The results highlighted the key role played by the Moho geometry, particularly as a step of ~10 km occurs between the Adriatic Moho of the subducting plate to the west and the new Tyrrhenian Moho characterizing the back-arc area to the west. The comparison between our results and available borehole data suggests a good fit between the applied analytical methodology and published datasets. A visible anomaly is located at a specific site (i.e., the coastal town of Senigallia), where it may be envisaged that fluid circulation produced a local surface heat flow increase; this makes the Senigallia area a promising feature for the possible exploitation of geothermal systems.

Keywords: central Italy; heat flow; 3D thermal modelling; thermal structure; temperature profile

Citation: Santini, S.; Basilici, M.; Invernizzi, C.; Jablonska, D.; Mazzoli, S.; Megna, A.; Pierantoni, P.P. Controls of Radiogenic Heat and Moho Geometry on the Thermal Setting of the Marche Region (Central Italy): An Analytical 3D Geothermal Model. *Energies* **2021**, *14*, 6511. https://doi.org/10.3390/en14206511

Academic Editor: Carlo Roselli

Received: 25 August 2021
Accepted: 4 October 2021
Published: 11 October 2021

1. Introduction

The high geothermal energy potential is well known in central Italy, especially in the Tuscany region, where geothermal exploration started during the 1990s in Larderello and Monte Amiata [1–6]. At present, closer attention has been given to the geothermal energy potential of the neighboring Marche region, involving the investigation of both fluid circulation [7] and surface heat flux [8–10]. Recent studies focused on the central Apennines regional setting, which is characterized by an increasing surface heat flow moving from the mountain chain to the Adriatic off-shore to the east, besides that occurring toward the Tuscany region to the west [8–10].

When assessing a potential site for geothermal exploitation, a comprehensive picture of crustal setting and temperature profile is fundamental for any site-specific, appropriate field development. Today, indispensable geothermal suitability assessments are often carried out using a series of invasive inspections involving legal permission and high cost (e.g., well drilling) [11].

In this study, we produced the first 3D geological model of the crust in the Marche region based on Moho depth provided by Grad et al. [12], the seismic profile CROP-03 interpreted by Barchi et al. [13] and Santini et al. [9], a series of published balanced geological cross-sections [14–16], the geological map by Conti et al. [17] and a 10 m cell

size digital elevation model (DEM) [18]. Subsequently, taking into account the heat rising from the mantle and the radiogenic heat produced by radioactive elements in the crust, an analytical methodology was used in order to produce a crustal 3D thermal model of the entire sector based on the pre-built 3D geological model. Finally, we compared our results with those obtained by previous studies to improve the description of thermal implications. This work provides a general framework of temperature distributions in the studied area, and emphasizes the key role played by the Moho geometry in the thermal structure of the central Apennines.

2. Geological Background

The area of study (Figure 1) is located in the Apennine fold and thrust belt. This area represents the most recent expression of the geodynamic process that produced the Mediterranean basins after the collision between Europe and Africa, which started during the late Cretaceous period and was followed by Oligocene and Neogene periods' slab-retreat events [15,17,19–22].

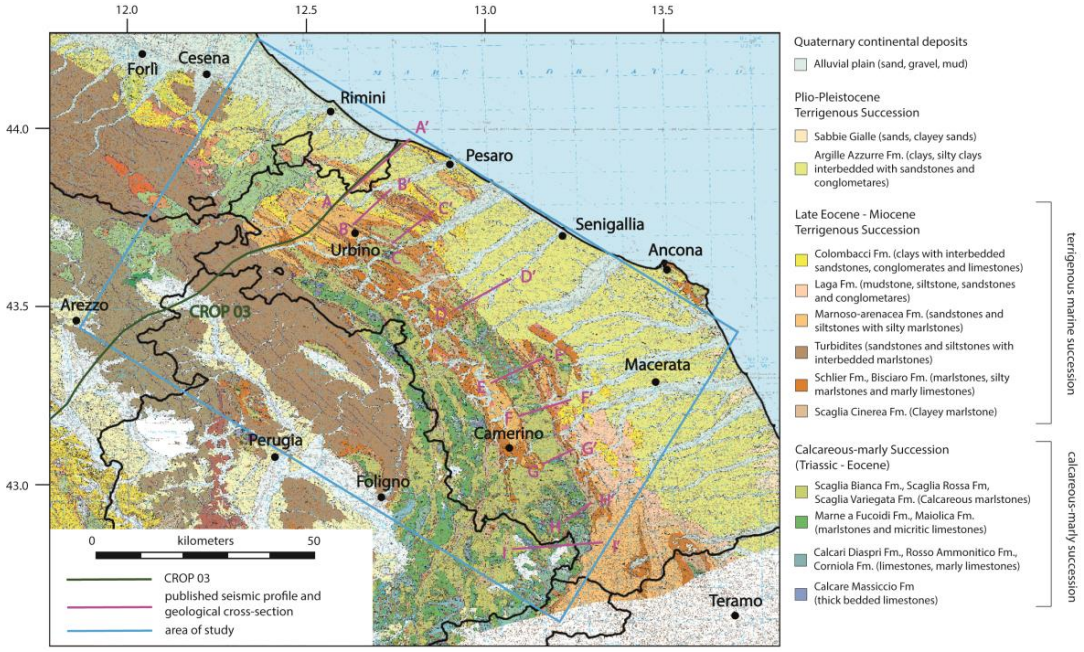

Figure 1. Area of study (blue rectangle). The green line is the trace of the seismic profile CROP-03 [13], the violet lines are the published balanced geological cross-sections [14–16]. The base is the geological map after Conti et al. [17].

The tectonic evolution of the entire area is strongly debated due to the complexity of the geodynamic processes that generated the mountain chain (e.g., [9,21,23,24]). Several authors have proposed models based on stratigraphic and structural analysis of transects oriented along the flow lines of relative motion [25,26], whereas others have followed an approach based on the laws of plate kinematics [22,27]; however, all of these studies found a Moho step in correspondence with the Apennines chain, caused by a discontinuity between the subducting Adriatic plate and the Tyrrhenian back-arc domain to the west. The Moho step (~10 km) was also observed by recent geophysical studies of Italian and European Moho geometry [12,21,28–33].

In this study area, the deepest units are the Paleozoic crystalline basement and the overlaying Permo-Triassic continental siliciclastic strata (i.e., the Verrucano Group). Neither of them crop out in the area, but their presence was confirmed by seismic studies and deep wells [28,34]. The overlying sedimentary cover is several thousand meters thick. It is composed of Triassic evaporites (Burano Anhydrites Fm.) followed by the ca. 1000 m thick, pre-orogenic and dominantly carbonate, Triassic–Eocene portion of the Umbria–Marche succession (including the Calcare Massiccio Fm. at the base, up to the Scaglia Rossa Fm.

at the top). This is overlain by a 2000–2500 m thick succession of Late Eocene to Plio-Pleistocene, dominantly terrigenous marine deposits (including the Scaglia Cinerea Fm. up to the Sabbie Gialle Fm.), followed by late Quaternary continental deposits (Figure 1) [35–38].

Overlying the Triassic evaporites, the Late Triassic–Lower Jurassic platform carbonates of the Calcare Massiccio Fm. reach 800 m of thickness. During the Jurassic extensional phase, the carbonate platform was dissected by normal faults, producing structural depressions and structural heights [39]. On this uneven bathymetry, pelagic sediments of variable thickness were deposited forming 'complete', 'condensed' and 'composite' successions [40,41]. Basin deposition of limestone and marl continued from Late Jurassic to Middle Miocene times, progressively increasing the contribution of argillaceous material in younger formations. The closure of the Mesozoic Tethys Ocean and the collision of European (Corsica–Sardinia block) and African (Adria block) continental margins, resulted in collisional orogenesis since the Oligocene [42]. The resulting fold-and-thrust belt consists of ENE-verging folds and WSW-dipping thrusts [14–16,43–49]. Coeval deposition of siliciclastic material occurred in the evolving foreland basin system (including, in the Marche region, the Miocene–Arenacea, Camerino and Laga basins [50], as well as the Plio-Pleistocene Argille Azzurre basin (stratigraphically overlying Messinian evaporites). Late Quaternary continental deposits unconformably overly the marine succession.

The stress field acting in the axial zone of the central Apennines since the Middle Pleistocene produced normal fault systems responsible for moderate to high seismicity [51,52] in the inner zone of the Marche region [16,53–66], whereas active horizontal compression characterizes the coastal sector and offshore areas [67,68].

3. Materials and Methods

In order to produce a 3D geothermal model of the Marche region, we used an analytical procedure based on a 3D geological model and calculated geotherms on a series of pseudo-wells located within the 3D geological model. The results for each pseudo-well were then interpolated to produce a 3D model of the entire thermal structure of the region.

3.1. 3D Geological Model

Over the years, many authors produced geological cross-sections perpendicular to the strike of the mountain chain based on available seismic profiles and geological field observations [7,13–16,21,49,69]. Furthermore, seismic tomographies were performed to investigate the thickness of the sedimentary cover and the Moho depth [12,21,29,31–33].

We produced a three-layer 3D geological model of the study area based on the Moho geometry provided by Grad et al. [12], the inner zone of the seismic profile CROP-03 [13] interpreted by Mazzoli et al. [14] (Figure 2), a series of published balanced geological cross-sections [14–16] (Figure 3), the geological map by Conti et al. [17] (Figure 1), and a 10 m cell size digital elevation model (DEM) [18].

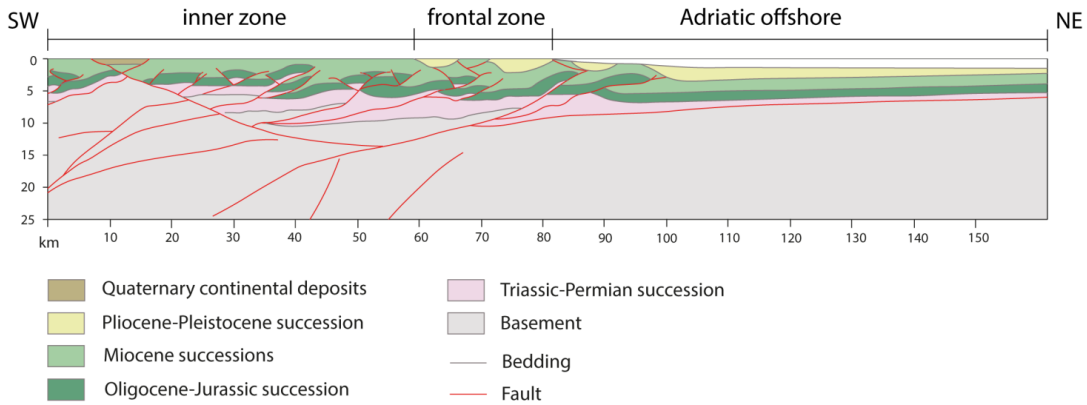

Figure 2. CROP-03 profile interpreted by Barchi et al. [13] (onshore) collated with offshore sector by Santini et al. [9].

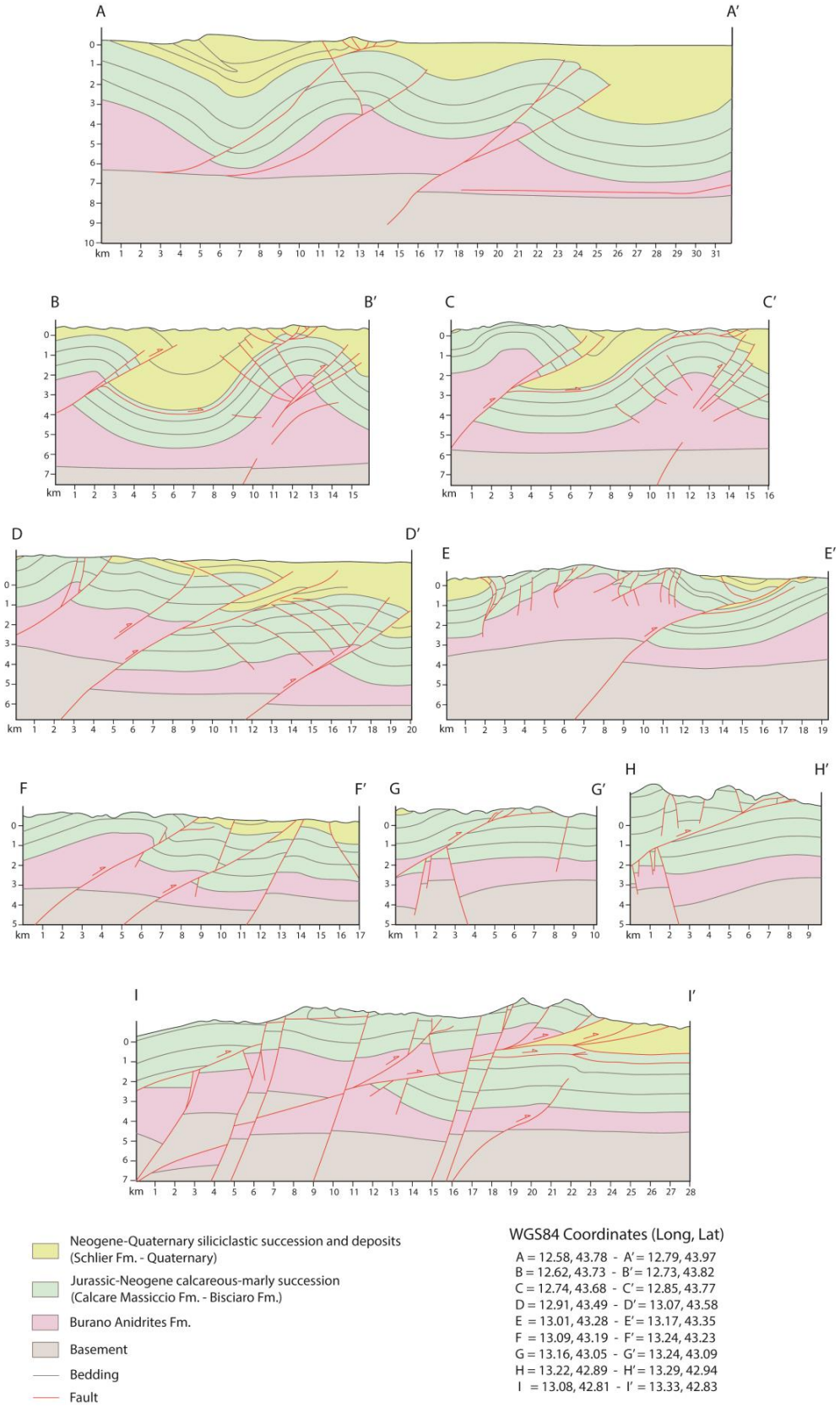

Figure 3. Published balanced geological cross-sections, with WGS84 coordinates [14–16].

The three-layer 3D geological model (Figure 4) was built using Blender [70], a free and open-source 3D computer graphics software used to show complex 3D geometries in many fields of study [71,72], including geology and geophysics [73–75].

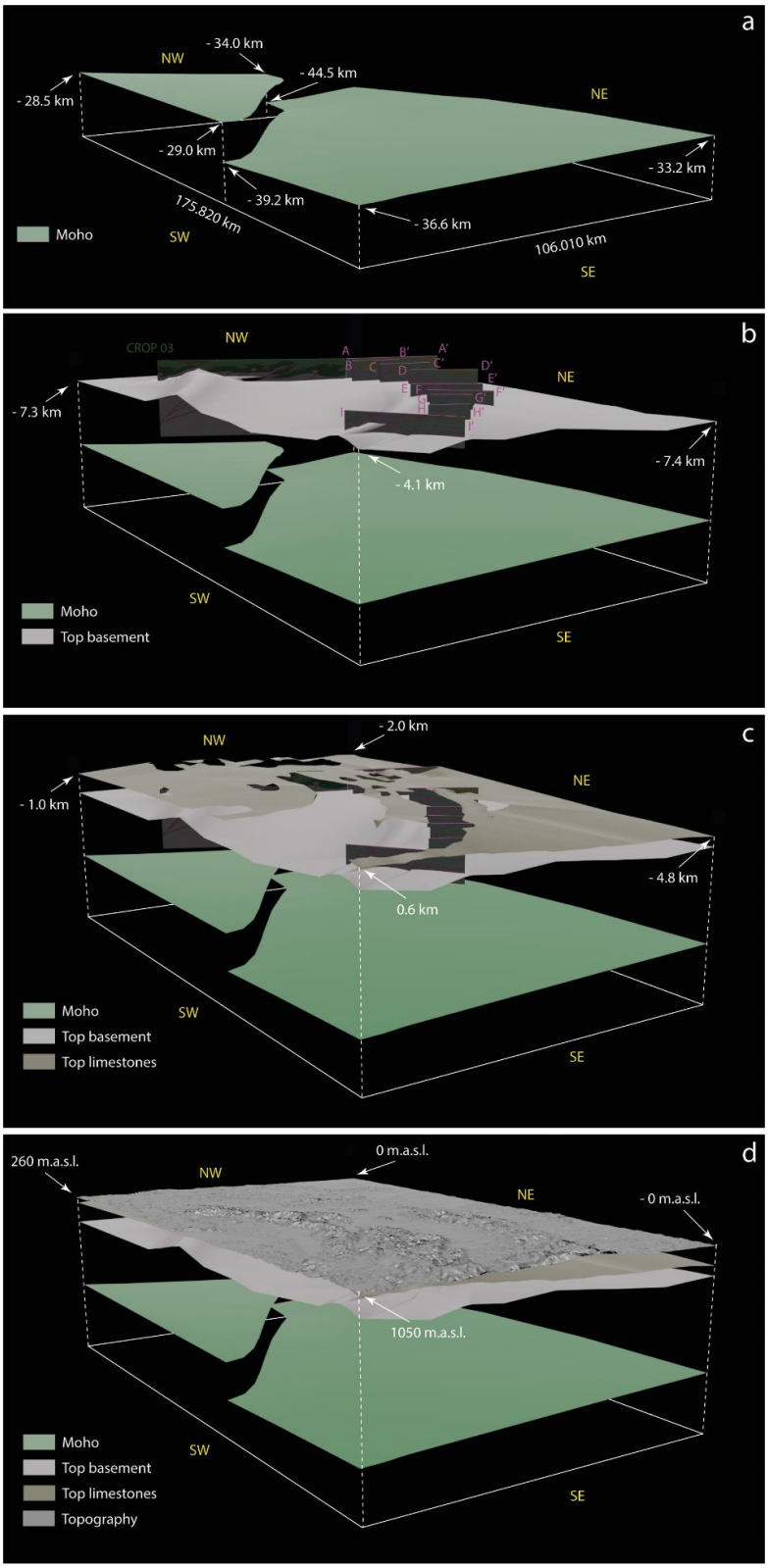

Figure 4. Geological 3D model of the area of study (152.245 km × 98.930 km): (**a**) 3D Moho based on Grad et al. [12]; (**b**) Top basement surface based on CROP-03 [13] interpreted by Mazzoli et al. [14] and published balanced geological cross-section [14–16]; (**c**) Top limestones surface based on CROP-03 [12] interpreted by Mazzoli et al. [14], published balanced geological cross-section [14–16] and geological map of Conti et al. [17]; (**d**) Complete 3D geological model composed by Moho, top basement, top limestones and topography based on a 10 m cell size digital elevation model (DEM) [18].

3.2. Geothermal Model: Constraints and Assumptions

The computational procedure took into account the heat rising from the mantle and the radiogenic heat due to radioactive elements located in the crust. The latter is divided, in this case, into three layers (Figure 4). To perform the geothermal model, we considered one hundred and sixty-five pseudo-wells located in the nodes of a ca. 10 × 10 km sampling grid traced on the study area, in addition to other six pseudo-wells placed on CROP-03 (Figure 5).

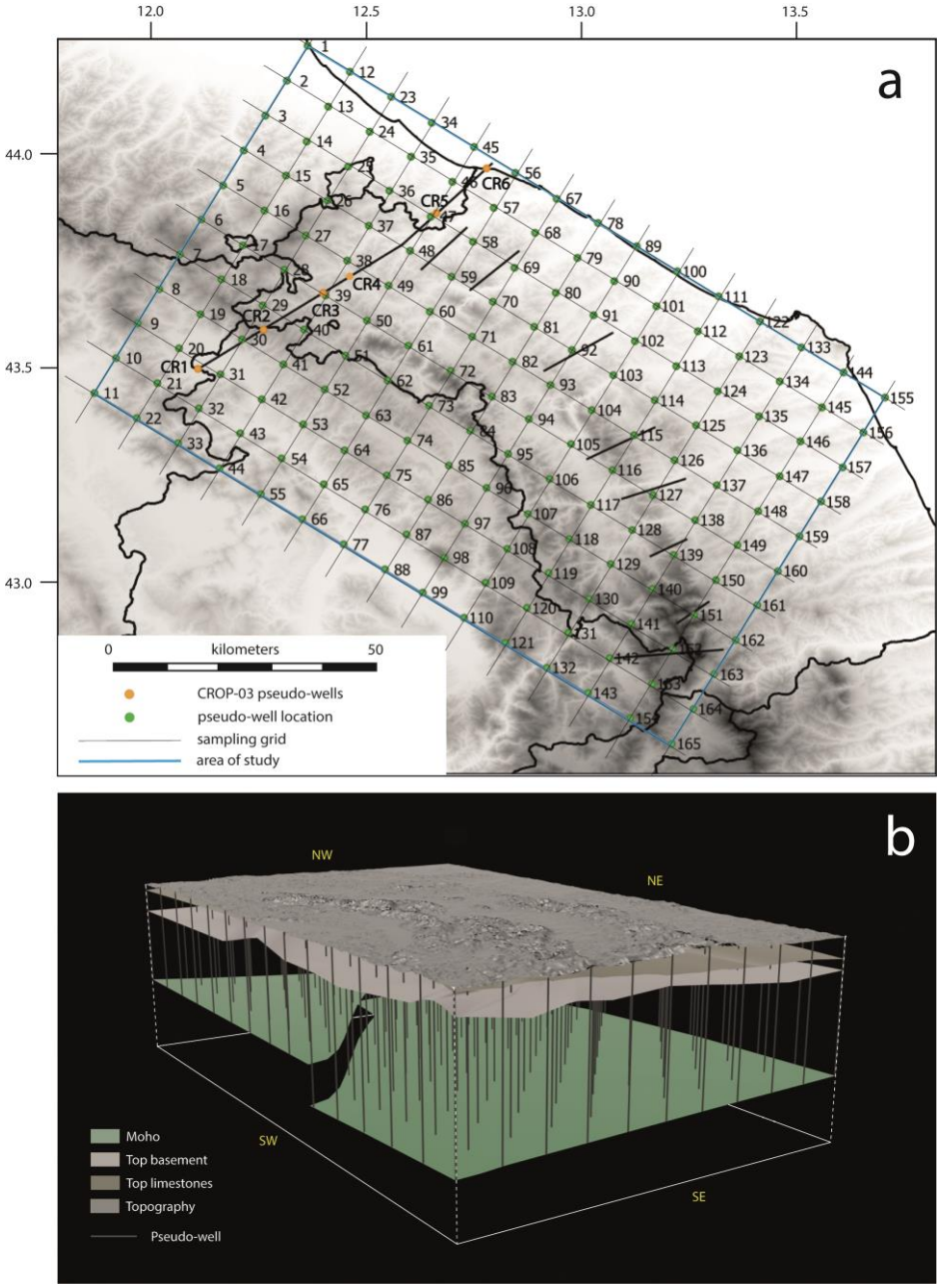

Figure 5. (**a**) Map view of the sampling grid with one hundred and sixty-five pseudo-wells and the other six (from CR1 to CR6) placed on CROP-03; (**b**) 3D geological model with pseudo-wells.

Each pseudo-well included data on the heat source, Moho depth, and thickness of each layer considering:

1 Altitude: we took into account the topography using a 10 m cell size digital elevation model (DEM) [18];

2 Variable thickness of the first layer (h_{CS}) represented the terrigenous marine succession (Late Eocene to Plio-Pleistocene) and late Quaternary continental deposits. It was based on a series of published balanced geological cross-sections [14–16] (Figure 3), and the geological map by Conti et al. [17] (Figure 1). We considered a constant heat production rate of the Siliciclastic succession $H_{CS} = 1.05$ μWm^{-3} (with a range of 0.9–1.3 μWm^{-3}) [10] and thermal conductivity $k_{CS} = 2.1$ Wm^{-1} °C^{-1} (with a range of 2.0–2.2 Wm^{-1} °C^{-1}) [8];

3 The variable thickness of the second layer (h_{CC}), representing the Umbria–Marche calcareous–marly succession from Triassic evaporites (Burano Anhydrites Formation) to the Scaglia Rossa Fm., was based on a series of published balanced geological cross-sections [14–16] (Figure 3), and the geological map by Conti et al. [17] (Figure 1). We considered the constant heat production rate of the Umbria–Marche calcareous–marly succession, $H_{CC} = 0.45$ μWm^{-3} (with a range of 0.3–0.6 μWm^{-3}) [10], and thermal conductivity, $k_{CC} = 2.4$ Wm^{-1} °C^{-1} (with a range of 2.3–2.5 Wm^{-1} °C^{-1}) [8];

4 Variable thickness of the third layer (h_B) represented the basement. We considered a thickness of the basement from the Moho (based on Grad et al. [12]) to the top basement constrained by the CROP-03 seismic profile [13] interpreted by Mazzoli et al. [14] (Figure 2) and a series of published balanced geological cross-sections [14–16] (Figure 3). We considered a basement thermal conductivity of $k_B = 2.7$ Wm^{-1} °C^{-1} (with a range of $2.6 - 2.8$ Wm^{-1} °C^{-1}) [8] and a heat production rate of the basement of $H_B = 3.15$ μWm^{-3} (with a range of $3.0 - 3.3$ μWm^{-3}) [76,77], exponentially decreasing with depth. The radiogenic sources' intensity, for any thickness h_B, diminished downward with a logarithmic decrement D, which had the dimension of depth and a characteristic value of 8 km in the region [76,78];

5 Variable heat flux at the Moho (Q_m) from 20 mWm^{-2} to the east and 40 mWm^{-2} to the west [21,79,80].

3.3. Analytical Procedure

The entire thermal structure is affected by two sources of heat: (i) the heat flowing upward from the Moho, coming from the mantle (Q_m), and (ii) the heat production rates of the cover (H_{CS} and H_{CC}) and the basement (H_B), due to the presence of radioactive elements in the crust. To obtain the surface heat flux, we used the analytical procedure by Dragoni et al. [76] and further applied by Santini et al. [9,78] and Basilici et al. [74,81], modified specifically for the area of study. In the computation of the surface heat flow, in addition to contributions of Q_m, we added radiogenic heat, obtaining the following equation used to calculate the surface heat flow (Q_s):

$$Q_S = Q_m + H_{CS}h_{CS} + H_{CC}h_{CC} + H_B D\left(1 - e^{-\frac{(h-h_C)}{D}}\right) \quad (1)$$

where h and h_C are the thicknesses of the crustal structure and of the whole cover, respectively, with $h_C = h_{CS} + h_{CC}$.

To compute the temperature trend with the depth, we adopted the analytical procedure summarized in Table 1, while the parameters considered are listed in Table 2 (with symbols and related definitions).

Table 1. Equations adopted for the analytical procedure.

	$0 \leq z \leq h_{CS}$	$h_{CS} < z \leq h_C$	$h_C < z \leq h$
$T(z)$	$T_s + T_{CSH}(z)$	$T_s + T_{CSH}(h_{CS}) + T_{CCH}(z)$	$T_s + T_{CSH}(h_{CS}) + T_{CCH}(h_C) + T_{BH}(z)$
$T_{CSH}(z)$	$\frac{Q_S}{k_{CS}} z - \frac{H_{CS}}{2k_{CS}} z^2$		
$T_{CCH}(z)$		$\frac{Q_S - H_{CS} h_{CS}}{k_{CC}} (z - h_{CS}) - \frac{H_{CC}}{2k_{CC}} (z - h_{CS})^2$	
$T_{BH}(z)$			$\frac{Q_m}{k_B} (z - h_C) + \frac{H_B D^2}{k_B} \left(1 - e^{-\frac{(z-h_C)}{D}}\right)$

Table 2. Analytical procedure parameters.

h_{CC}	calcareous cover thickness
h_C	whole cover thickness
h_B	basement thickness
h	whole crustal thickness
D	depth scale
H_{CS}	siliciclastic cover radioactivity produced heat
H_{CC}	calcareous cover radioactivity produced heat
H_B	basement radioactivity produced heat
k_{CS}	siliciclastic cover thermal conductivity
k_{CC}	calcareous cover thermal conductivity
k_B	basement thermal conductivity
Q_s	surface heat flow density
Q_m	mantle heat flow density
T_s	surface temperature
T_{CSH}	siliciclastic cover heat temperature
T_{CCH}	calcareous cover heat temperature
T_{BH}	basement heat temperature
h_{CS}	siliciclastic cover thickness

The temperature in the first layer (h_{CS}) is due to the heat flow at the top of calcareous cover and to the contribution of the radiogenic source of this layer, adding to these, the surface temperature (T_S)

$$T(z) = T_S + \frac{Q_S}{k_{CS}} z - \frac{H_{CS}}{2k_{CS}} z^2,\ 0 \leq z \leq h_{CS} \tag{2}$$

for simplicity, defining the depth dependent terms as $T_{CSH}(z)$.

In the second layer (h_{CC}), the geotherm initial value is the temperature at the bottom of the first layer $(T_S + T_{CSH}(h_{CS}))$, to which is added the temperature variation due to the radiogenic source present in the calcareous cover and to the heat flow at its bottom

$$T(z) = T_S + T_{CSH}(h_{CS}) + \frac{Q_S - H_{CS} h_{CS}}{k_{CC}} (z - h_{CS}) - \frac{H_{CC}}{2k_{CC}} (z - h_{CS})^2, h_{CS} \leq z \leq h_C \tag{3}$$

defining the depth dependent terms as $T_{CCH}(z)$.

Finally, the temperature in the basement depends on the mantle heat flow and on the radiogenic source present in it, adding the temperature calculated at the top of the layer $(T_s + T_{CSH}(h_{CS}) + T_{CCH}(h_C))$

$$T(z) = T_S + T_{CSH}(h_{CS}) + T_{CCH}(h_C) + \frac{Q_m}{k_B} (z - h_C) + \frac{H_B D^2}{k_B} \left(1 - e^{-\frac{(z-h_C)}{D}}\right), h_C \leq z \leq h \tag{4}$$

4. Results

Using the analytical procedure described in Section 3.3, we calculated surface heat flow, geotherms, and isotherms for each pseudo-well (Figure 5) located in the 3D geological model (Figure 4). The output model of the surface heat flow computation is shown in

Figure 6. It was obtained by interpolating the Q_S value obtained from each pseudo-well with a fourth-order polynomial equation.

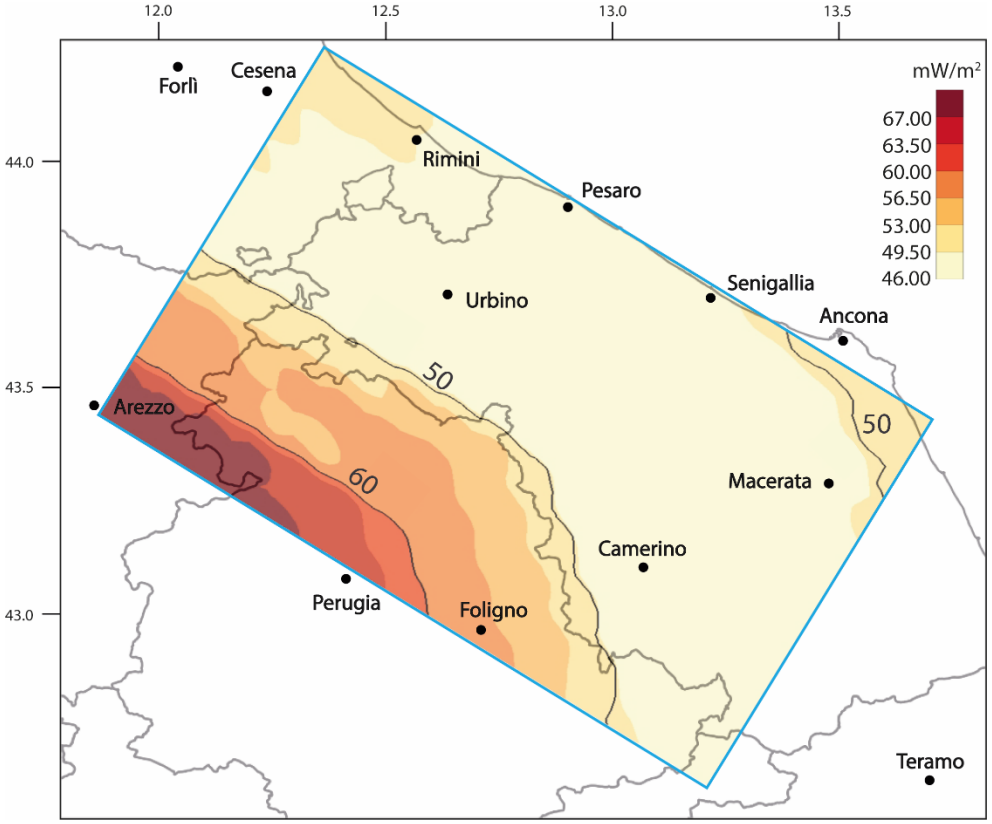

Figure 6. Surface heat flow obtained interpolating the surface heat flow value resulted by each pseudo-well with a fourth-order polynomial equation.

The variable thickness of the three layers of the 3D geological model produced a variable trend in the surface heat flow, which appears to be strongly influenced by the Moho geometry. Surface heat flow varies from 46–50 mWm^{-2} in the central zone, to 60–67 mWm^{-2} in the inner zone (Arezzo–Perugia area). This variation appears to be mainly associated with the Moho step, which rises the top of the mantle by ~10 km in the SW sector (Figure 4a). In addition, the Rimini–Cesena area and the zone located between Ancona and Macerata, show an increase in surface heat flow of ~5 mWm^{-2}, probably due to the thickening of the Siliciclastic succession (Figure 4b,c). Furthermore, considering the range of values of the radiogenic heat sources for the three layers, we estimated the changes in the computed surface heat flow. In particular, we obtained a maximum increase of about 6% if the upper limits of the range are considered, whereas the decrease in surface heat flow did not exceed 5%, taking into account the lower limits of the range.

To study the trend in the temperature and depth along the CROP-03 line, we calculated the geotherms for the six pseudo-wells located along the profile, and then interpolated them using second-order polynomial equations representing the 50°, 100°, 150° and 200° isotherms. Figures 7 and 8 show the geotherms calculated for the pseudo-wells CR1 to CR6 (Figure 5) and the relative isotherms along the CROP-03 (Figure 2), respectively. In particular, pseudo-well CR2 showed an overall higher temperature profile with respect to CR1 (Figure 7). This was due to the higher altitude (of 1000 m a.s.l.) of CR1 with respect to the other pseudo-wells (located 0–400 m a.s.l.). Nevertheless, the general trend in the calculated geotherms and interpolated isotherms shows an increase in the temperature gradient going from the coastal area to the inner zone.

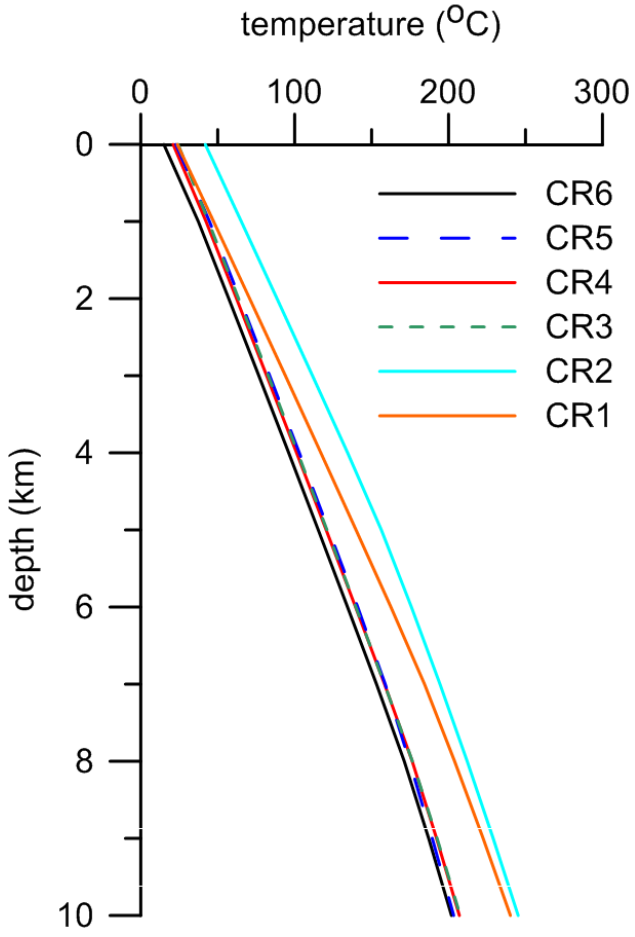

Figure 7. Calculated geotherms relative to the pseudo-wells from CR1 to CR6 along the CROP-03 of Figure 3.

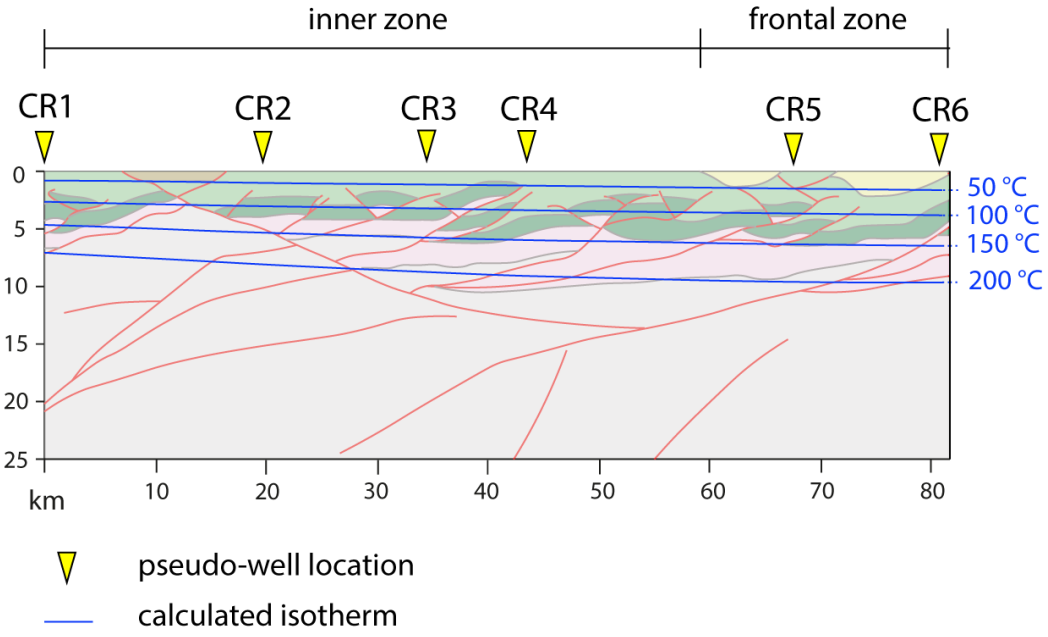

Figure 8. Isotherms interpolated by a second-order polynomial equation along the inner and frontal zones of the CROP-03 (Figure 3) using the geotherms relative to pseudo-wells from CR1 to CR6. Black symbols indicate the calculated temperatures of 50 °C, 100 °C, 150 °C and 200 °C.

Furthermore, in order to analyze the trend in the isotherms for the whole study area, we calculated the geotherm for each pseudo-well, and then interpolating by second-order polynomial equations, we obtained the contour maps representing the 50 °C, 100 °C, 150 °C and 200 °C isotherms (Figure 9). The contour map for the isotherm at 50 °C shows a general, northward deepening trend characterized by an area of shallow depth (<1.1 km), south of Camerino. On the other hand, the isotherm 100 °C map shows a dominantly north-eastward deepening trend, with its shallowest depths in the westernmost area (close to Arezzo). The contour maps of 150 °C and 200 °C isotherms show similar trends characterized by greater depths in a wider area—defined as a 'thermal depression'—extending from Pesaro to Camerino and just west of Macerata, whereas the shallowest depths occur in the westernmost area (close to Arezzo and Perugia).

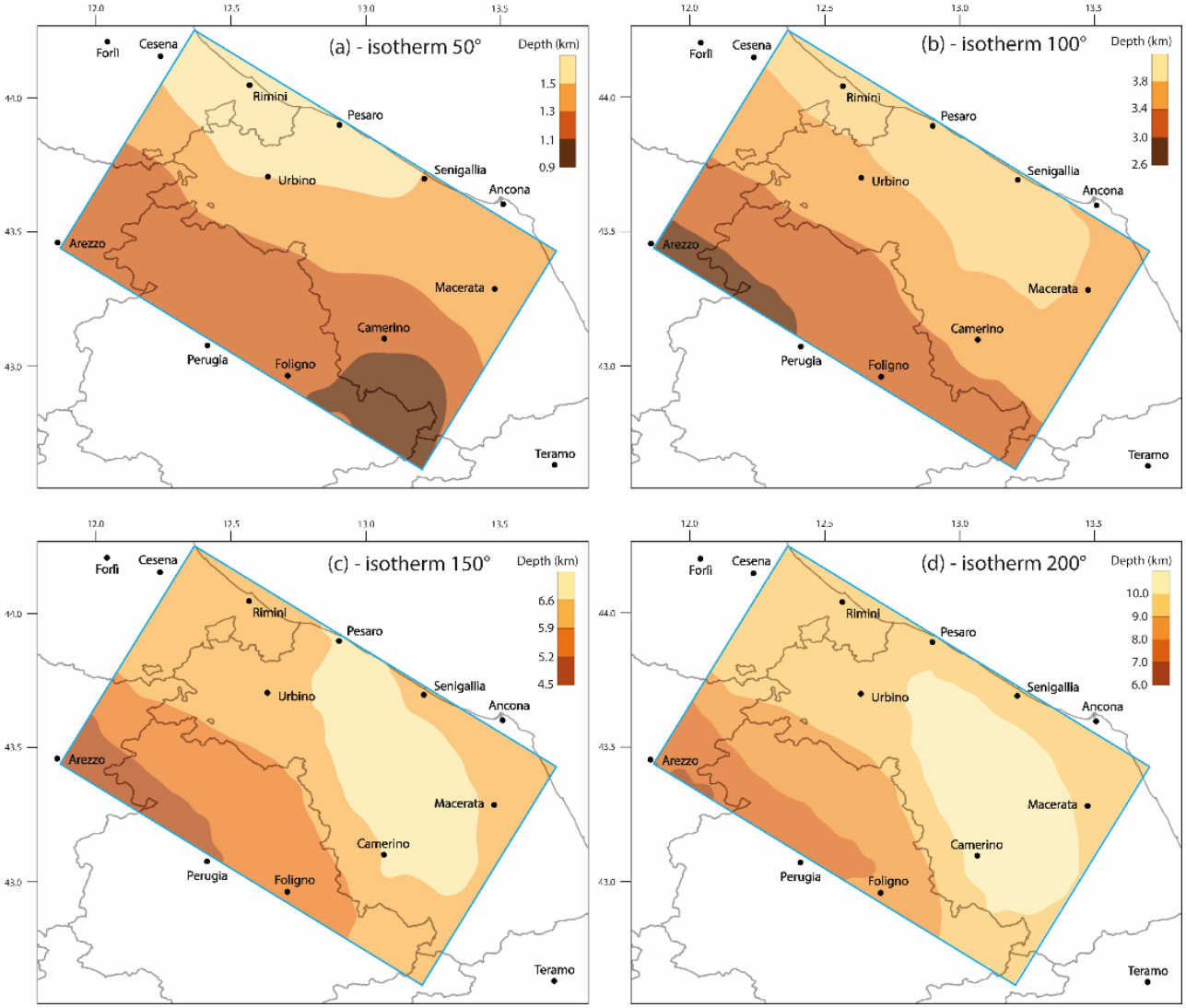

Figure 9. Isotherm depth contour maps obtained by second-order polynomial equation interpolation for the (**a**) 50 °C, (**b**) 100 °C, (**c**) 150 °C and (**d**) 200 °C isotherms.

5. Discussion

The thermal structure of the area is characterized by a trend that highlights a general increase in temperature from the coastal area to the inner zone. This is visible in the model of the surface heat flow (Figure 6), along the CROP-03 profile (Figures 7 and 8) and in the temperature contour map (Figure 9). The analytical procedure indicates that the geometry of the Moho produces a high impact on the entire thermal setting of the Marche region,

showing high heat flow values where the Moho is shallower (Arezzo–Perugia–Foligno area) and a sharp decrease in heat flow values, corresponding to the ~10 km Moho step. The presence of radioactive elements in the crust, instead, produces a homogeneous increase in temperature in the entire area, especially where the siliciclastic layer increases in thickness. However, the difference in the heat production rates between the calcareous layer ($H_{CC} = 0.45$ μWm^{-3}) and the siliciclastic layer ($H_{CS} = 1.05$ mWm^{-3}) is substantial. A difference of 0.60 mWm^{-3} in the heat production rate is also responsible for the 'thermal depression' located between Pesaro, Camerino and Macerata, where the siliciclastic cover is almost absent. On the other hand, the rise of the 50 °C isotherm south of Camerino could be linked with the circulation and ascent towards the surface of fluids in correspondence with the most important calcareous reliefs.

To obtain a better understanding of the thermal structure of the study area, our results were compared with previous studies [8,10,82]. Pauselli et al. [10] produced a surface heat flow map of central Italy constrained by available thermal and petrophysical logs from wells drilled for geothermal and hydrocarbon exploration purposes. In Figure 10, we compared our surface heat flow map with the results of Pauselli et al. [10].

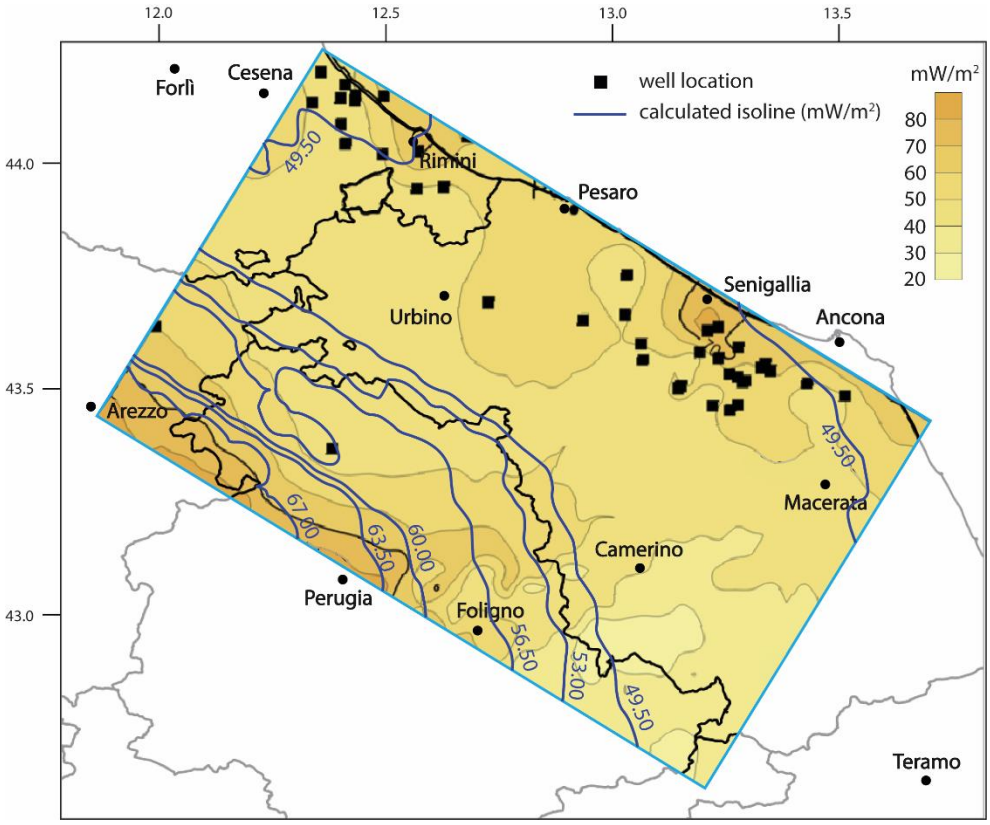

Figure 10. Heat flow map by Pauselli et al. [10] compared with calculated surface heat flow map (Q_S) shown in Figure 7 (blue lines).

The general trend in the surface heat flow calculated by the improved analytical procedure is comparable with that obtained by Pauselli et al. [10]. The Arezzo–Perugia area represents the highest value of Q_S in the entire region (~70 mWm^{-2}) in both our study (Figure 6) and in Pauselli et al. [10] (Figure 10). Slightly more elevated values in the map created by Pauselli et al. [10], with respect to our result, suggest a possible source of heat that is in addition to the radiogenic heat produced by the crust and the heat flowing up from the mantle (Q_m), which are included in the analytical procedure. In the Senigallia area, a Q_S discrepancy value is clear. This means that in Senigallia, the surface heat flow measured from the wells (Figure 10) is due to another heat source. Chicco et al. [7] highlighted the presence of deep, high-angle faults that can certainly influence fluid circulation by means

of water ascent from depth along fault damage zones. This fact makes the Senigallia area a promising feature for possible geothermal systems. Other Q_S discrepancies occur in the Rimini area, although they are less prominent. The rest of the map does not show Q_S discrepancies, thus confirming that most of the measured surface heat flow is due to the radiogenic heat and the heat flowing up from the mantle, which, in turn, depends on Moho geometry. This fact is visible in the Camerino–Pesaro area, where the absence of the siliciclastic cover results in a lower Q_S value in both the analytical model (our results, Figure 6) and measured values (Pauselli et al. [10] result, Figure 10).

Della Vedova et al. [8] computed isotherms along the CROP-03 profile using boreholes within a 10 km distance from the section trace and lithology-dependent thermal conductivity values. The result of the work is compared with our results in Figure 11.

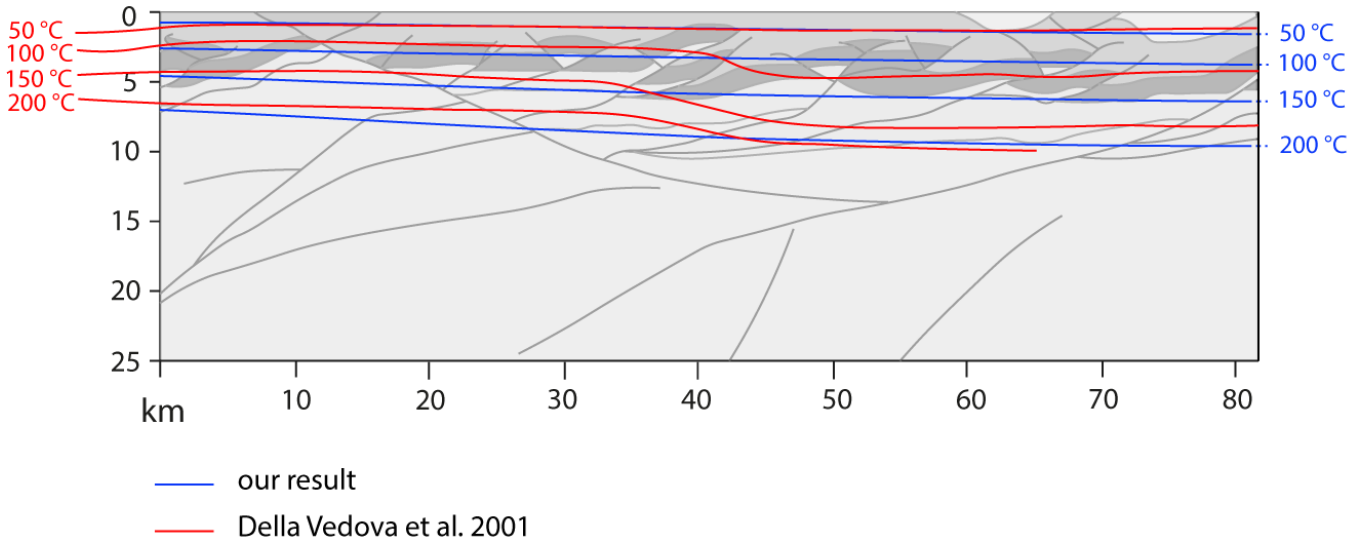

Figure 11. Calculated isotherms (in blue) compared with that by Della Vedova et al. [8] (in red).

The general trend pointed out by the analytical procedure (blue isotherms in Figure 11) is consistent with the results by Della Vedova et al. [8]. The temperature values discrepancy is probably due to a different mathematical interpolation used. Obviously, the T value discrepancy increases with depth. To improve the description of our results, in Figure 12, we compared three well temperature profiles published by Pauselli et al. [10], Della Vedova et al. [8] and Verdoja et al. [81] with the closest pseudo-wells of our study.

The comparison between our pseudo-wells (orange lines in Figure 12) and published temperature profiles (green lines in Figure 12) shows a good fit between the analytical model and borehole measurements.

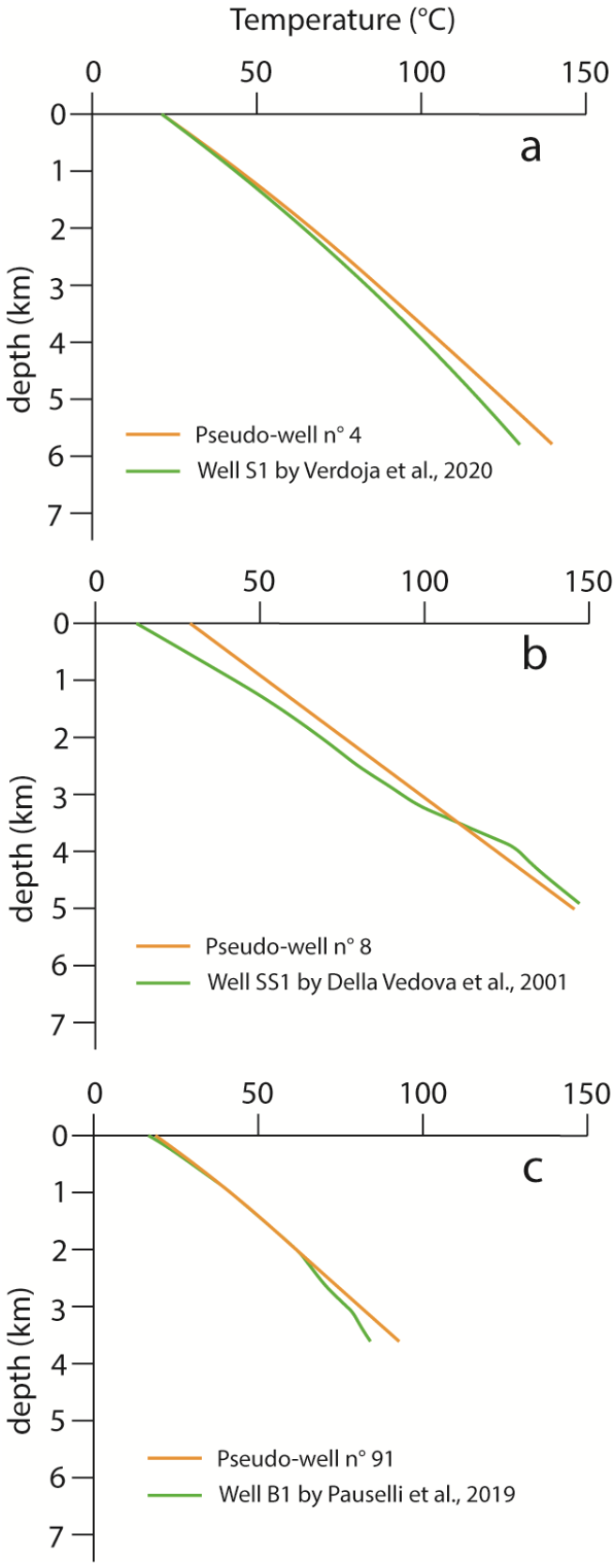

Figure 12. Comparison of the temperatures between (**a**) pseudo-well n° 4 and well Sarsina1 (S1) by Verdoja et al. [81], (**b**) pseudo-well n° 8 and well SS1 by Della Vedova et al. [8], (**c**) pseudo-well n° 91 and well B1 by Pauselli et al. [10].

6. Conclusions

The results of this study provide the first 3D geological model of the crust in the Marche region, based on Moho depth by Grad et al. [12], the deep seismic reflection profile CROP-03 [13] interpreted by Mazzoli et al. [14], a series of published balanced geological cross-sections [14–16], the geological map by Conti et al. [17] and a 10 m cell size digital elevation model (DEM) [18]. An analytical methodology was elaborated to produce a 3D geothermal model of the crust taking into account the heat rising from the mantle and the radiogenic heat produced by radioactive elements. The model output showed an increase in temperature going from the coastal area to the inner zone. Comparing our outcomes with published results of previous works [8,10,81], we highlighted compatible results between our model and borehole measurements. The Moho geometry appeared to play a key role in the temperature model of the entire Marche region, producing a sharp change in temperature where a step of ~10 km occurs between the Adriatic foreland and Tyrrhenian back-arc domains. In the Senigallia and Rimini areas, a discrepancy of surface heat flow occurred between our Q_S values and those provided by Pauselli et al. [10], probably due to circulating and rising fluids [7] not considered in the applied analytical procedure; this fact makes the Senigallia area a promising site to evaluate possible geothermal systems. In particular, besides the suitable condition for low-enthalpy plants for the heating/cooling of buildings, dedicated studies should be aimed at investigating the possibility of medium-enthalpy system plants.

Author Contributions: Conceptualization, S.S., M.B., S.M. and A.M.; methodology, S.S., M.B. and A.M.; software, M.B. and A.M.; validation, S.S., M.B., S.M. and A.M.; formal analysis, S.S. and A.M.; investigation, S.S., M.B., D.J. and P.P.P.; resources, D.J., S.M. and P.P.P.; data curation, M.B. and A.M.; writing—original draft preparation, M.B. and D.J.; writing—review and editing, S.S., C.I., A.M. and P.P.P.; visualization, M.B.; supervision, S.S., C.I. and S.M.; project administration, S.S. and S.M.; funding acquisition, S.S. and S.M. All authors have read and agreed to the published version of the manuscript.

Funding: This research received no external funding.

Informed Consent Statement: Not applicable.

Acknowledgments: The authors are grateful to the Editor for his support in organizing the manuscript. We thank two anonymous Reviewers for their useful comments and for their compliments.

Conflicts of Interest: The authors declare no conflict of interest.

References

1. Della Vedova, B.; Marson, I.; Panza, G.F.; Suhadolc, P. Upper mantle properties of the Tuscan-Tyrrhenian area: A key for understanding the recent tectonic evolution of the Italian region. *Tectonophysics* **1991**, *195*, 311–318. [CrossRef]
2. Pandeli, E.; Bertini, G.; Castellucci, P. The Tectonic Wedges Complex of the Larderello area (Southern Tuscany—Italy). *Boll. Soc. Geol. Ital.* **1991**, *110*, 621–629.
3. Cameli, G.M.; Dini, I.; Liotta, D. Upper crustal structure of the Larderello geothermal field as a feature of post-collisional extensional tectonics (Southern Tuscany, Italy). *Tectonophysics* **1993**, *224*, 413–423. [CrossRef]
4. Gianelli, G.; Puxeddu, M.; Batini, F.; Bertini, G.; Dini, I.; Pandeli, E.; Nicolich, R. Geological model of a young volcano-plutonic system: The geothermal region of Monte Amiata (Tuscany, Italy). *Geothermics* **1988**, *17*, 719–734. [CrossRef]
5. Bertini, G.; Casini, M.; Gianelli, G.; Pandeli, E. Geological structure of a long-living geothermal system, Larderello, Italy. *Terra Nova* **2006**, *18*, 163–169. [CrossRef]
6. Bertini, G.; Cappetti, G.; Fiordalisi, A. Characteristics of Geothermal Fields in Italy. *Giornale di Geologia Applicata* **2005**, *1*, 247–254. [CrossRef]
7. Chicco, J.M.; Pierantoni, P.P.; Costa, M.; Invernizzi, C. Plio-Quaternary tectonics and possible implications for geothermal fluids in the Marche Region (Italy). *Tectonophysics* **2019**, *755*, 21–34. [CrossRef]
8. Della Vedova, B.; Bellani, S.; Pellis, G.; Squarci, P. Deep temperatures and surface heat flow distribution. In *Anatomy of an Orogen: The Apennines and Adjacent Mediterranean Basins*; Vai, F., Martini, I.P., Eds.; Springer: Berlin/Heidelberg, Germany, 2001; pp. 65–76. [CrossRef]
9. Santini, S.; Mazzoli, S.; Megna, A.; Candela, S. Thermal Structure of the Outer Northern Apennines along the CROP-03 Profile. *JGG* **2016**, *8*, 4. [CrossRef]

10. Pauselli, G.; Gola, G.; Mancinelli, P.; Trumpy, E.; Saccone, M.; Manzella, A.; Ranalli, G. A new surface heat flow map of the Northern Apennines between latitudes 42.5 and 44.5 N. *Geothermics* **2019**, *81*, 39–52. [CrossRef]
11. Moeck, I.S. Catalog of geothermal play types based on geologic controls. *Renew. Sustain. Energy Rev.* **2014**, *37*, 867–882. [CrossRef]
12. Grad, M.; Tiire, T.; ESC Working Group. The Moho depth map of the European Plate. *Geophys. J. Int.* **2009**, *176*, 279–292. [CrossRef]
13. Barchi, M.; Minelli, G.; Magnani, B.; Mazzotti, A. Line CROP 03: Northern Apennines. *Mem. Descr. Carta Geol. d'Ital.* **2003**, *LXII*, 127–136.
14. Mazzoli, S.; Pierantoni, P.P.; Borraccini, F.; Paltrinieri, W.; Deiana, G. Geometry, segmentation pattern and displacement variations along a major Apennine thrust zone, central Italy. *J. Struct. Geol.* **2005**, *27*, 1940–1953. [CrossRef]
15. Coward, M.P.; de Donatis, M.; Mazzoli, S.; Paltrinieri, W.; Wezel, F.C. Frontal part of the northern Apennines fold and thrust belt in the Romagna-Marche area (Italy): Shallow and deep structural styles. *Tectonics* **1999**, *18*, 559–574. [CrossRef]
16. Pierantoni, P.P.; Deiana, G.; Romano, A.; Paltrinieri, W.; Borraccini, F.; Mazzoli, S. Geometrie strutturali lungo la thrust zone del fronte montuoso umbro-marchigiano-sabino. *Boll. Soc. Geol. Ital.* **2005**, *124*, 395–411.
17. Conti, P.; Cornamusini, G.; Carmignani, L. An outline of the geology of the Northern Apennines (Italy), with geological map at 1:250,000 scale. *Ital. J. Geosci.* **2020**, *139*, 149–194. [CrossRef]
18. Tarquini, S.; Isola, I.; Favalli, M.; Battistini, A. *TINITALY, a Digital Elevation Model of Italy with a 10 meters Cell Size (Version 1.0) [Data Set]*; Istituto Nazionale di Geofisica e Vulcanologia: Roma, Italy, 2007. [CrossRef]
19. Dewey, J.F.; Helman, H.L.; Turco, E.; Hutton, D.H.W.; Knott, S.D. Kinematics of the western Mediterranean. In *Alpine Tectonics—An Overview*; Coward, M.P., Dietrich, D., Eds.; Geological Society Special Publication: London, UK, 1989; Volume 45, pp. 265–283.
20. Schettino, A.; Turco, E. Tectonic history of the western Tethys since the Late Triassic. *GSA Bulletin* **2011**, *123*, 89–105. [CrossRef]
21. Piana Agostinetti, N.; Faccenna, C. Deep Structure of Northern Apennines Subduction Orogen (Italy) as Revealed by a Joint Interpretation of Passive and Active Seismic Data. *Geophys. Res. Lett.* **2018**, *45*, 4017–4024. [CrossRef]
22. Turco, E.; Macchiavelli, C.; Penza, G.; Schettino, A.; Pierantoni, P.P. Kinematics of Deformable Blocks: Application to the Opening of the Tyrrhenian Basin and the Formation of the Apennine Chain. *Geosciences* **2021**, *11*, 177. [CrossRef]
23. Mazzoli, S.; Barkham, S.; Cello, G.; Gambini, R.; Mattioni, L.; Shiner, P.; Tondi, E. Reconstruction of continental margin architecture deformed by the contraction of the Lagonegro Basin, southern Apennines, Italy. *J. Geol. Soc. Lond.* **2001**, *158*, 309–319. [CrossRef]
24. Speranza, F.; Chiappini, M. Thick-skinned tectonics in the external Apennines, Italy: New evidence from magnetic anomaly analysis. *J. Geophys. Res. Solid Earth* **2002**, *107*, 2290. [CrossRef]
25. Malinverno, A.; Ryan, W.B.F. Extension in the Tyrrhenian Sea and shortening in the Apennines as result of arc migration driven by sinking of the lithosphere. *Tectonics* **1986**, *5*, 227–245. [CrossRef]
26. Le Breton, E.; Handy, M.R.; Molli, G.; Ustaszewski, K. Post-20 Ma motion of the Adriatic Plate: New constraints from surrounding orogens and implications for crust-mantle decoupling. *Tectonics* **2017**, *36*, 3135–3154. [CrossRef]
27. Rosenbaum, G.; Lister, G.S. Neogene and Quaternary rollback evolution of the Tyrrhenian Sea, the Apennines, and the Sicilian Maghrebides. *Tectonics* **2004**, *23*, 1–17. [CrossRef]
28. Mele, G.; Sandvol, E. Deep crustal roots beneath the northern Apennines inferred from teleseismic receiver functions. *Earth Planet. Sci. Lett.* **2003**, *211*, 69–78. [CrossRef]
29. Di Stefano, R.; Kissling, E.; Chiarabba, C.; Amato, A.; Giardini, D. Shallow subduction beneath Italy: Three-dimensional images of the Adriatic-European-Tyrrhenian lithosphere system based on high-quality P wave arrival times. *J. Geophys. Res. Solid Earth* **2009**, *114*, B05305. [CrossRef]
30. Mele, G.; di Luzio, E.; di Salvo, C. Mapping Moho depth variations in central Italy from Ps_{Moho}-P delay times: Evidence of an E-W transition in the Adriatic Moho at 42°N latitude. *Geochem. Geophys.* **2013**, *14*, 10. [CrossRef]
31. Spada, M.; Bianchi, I.; Kissling, E.; Piana Agostinetti, N.; Wiemer, S. Combining controlled-source seismology and receiver function information to derive 3-D Moho topography for Italy. *Geophys. J. Int.* **2013**, *194*, 1050–1068. [CrossRef]
32. Di Stefano, R.; Ciaccio, M.G. The lithosphere and asthenosphere system in Italy as inferred from the Vp and Vs 3D velocity model and Moho map. *J. Geodyn.* **2014**, *82*, 16–25. [CrossRef]
33. Gualtieri, L.; Serretti, P.; Morelli, A. Finite-difference P wave travel time seismic tomography of the crust and uppermost mantle in the Italian region. *Geochem. Geophys.* **2014**, *15*, 1. [CrossRef]
34. Anelli, L.; Gorza, M.; Pieri, M.; Riva, M. Subsurface well data in the Northern Apennines (Italy). *Mem. Soc. Geol. Ital.* **1994**, *48*, 461–471.
35. Martinis, B.; Pieri, M. Alcune nozioni sulla formazione evaporitica del Triassico Superiore nell'Italia centrale e meridionale. *Mem. Soc. Geol. Ital.* **1964**, *4*, 649–687.
36. Passeri, L. L'ambiente deposizionale della formazione evaporitica nel quadro della paleogeografia del Norico tosco-umbro-marchigiano. *Boll. Soc. Geol. Ital.* **1975**, *94*, 231–268.
37. Ciarapica, G.; Cirilli, S.; Passeri, L.; Trinciardi, E.; Zaninetti, L. "Anidriti di Burano" et "Formation du Monte Cetona" (nouvelle formation), biostratigraphie de deux-types du Trias supérieur dans l'Apennin septentrional. *Rev. Paléobiol.* **1985**, *2*, 341–409.
38. Centamore, E.; Cantalamessa, G.; Micarelli, A.; Potetti, M.; Berti, D.; Bigi, S.; Morelli, C.; Ridolfi, M. Stratigrafia e analisi di facies dei depositi del Miocene e del Pliocene inferiore dell'avanfossa marchigiano-abruzzese e delle zone limitrofe. *Studi Geologici Camerti* **1991**, *31*, 125–131.

39. Marchegiani, L.; Bertotti, G.; Cello, G.; Deiana, G.; Mazzoli, S.; Tondi, E. Pre-orogenic tectonics in the Umbria-Marche sector of the Afro-Adriatic continental margin. *Tectonophysics* **1999**, *315*, 123–143. [CrossRef]
40. Centamore, E.; Chiocchini, M.; Deiana, G.; Micarelli, A.; Pieruccini, U. Contributo alla conoscenza del Giurassico dell'Appennino Umbro-Marchigiano. *Studi Geologici Camerti* **1971**, *1*, 1–81.
41. Deiana, G.; Cello, G.; Chiocchini, M.; Galdenzi, S.; Mazzoli, S.; Pistolesi, E.; Potetti, M.; Romano, A.; Turco, E.; Principi, M. Tectonic evolution of the external zones of the Umbria-Marche Apennines in the Monte San Vicino-Cingoli area. *Boll. Soc. Geol. Ital.* **2002**, *1*, 229–238.
42. Carmignani, L.; Kligfield, R. Crustal extension in the Northern Apennines: The transition from compression to extension in the Alpi Apuane core complex. *Tectonics* **1990**, *9*, 1275–1303. [CrossRef]
43. Winter, T.; Tapponnier, P. Extension majeure post-Jurassique et ante-Miocène dans le centre de l'Italie: Donnèes microtectoniques. *Bull. Soc. Geol. Fr.* **1991**, *162*, 1095–1108.
44. Bally, A.W.; Burbi, L.; Cooper, C.; Ghelardoni, R. Balanced sections and seismic reflection profiles across the Central Apennines. *Mem. Soc. Geol. Ital.* **1986**, *35*, 257–310.
45. Menichetti, M.; Minelli, G. Extensional tectonics and seismogenesis in Umbria (Central Italy) The Gubbio Area. *Boll. Soc. Geol. Ital.* **1991**, *110*, 857–880.
46. Calamita, F.; Cello, G.; Deiana, G. Structural styles, chronology rates of deformation, and time-space relationships in the Umbria-Marche thrust system (central Apennines, Italy). *Tectonics* **1994**, *13*, 873–881. [CrossRef]
47. Ponziani, F.; de Franco, R.; Minelli, G.; Biella, G.; Federico, C.; Pialli, G. Crustal shortening and duplication of the Moho in the Northern Appennines: A view from seismic refraction data. *Tectonophysics* **1995**, *252*, 1–4. [CrossRef]
48. Chiappini, M.; Meloni, A.; Boschi, E.; Faggioni, O.; Beverini, N.; Carmisciano, C.; Marson, I. Shaded relief magnetic anomaly map of Italy and surrounding marine areas. *Annali di Geofisica* **2000**, *43*, 5.
49. Tozer, R.S.J.; Butler, R.W.H.; Chiappini, M.; Corrado, S.; Mazzoli, S.; Speranza, F. Testing thrust tectonic models at mountain fronts: Where has the displacement gone? *J. Geol. Soc. Lond.* **2006**, *163*, 1–14. [CrossRef]
50. Bigi, S.; Casero, P.; Ciotoli, G. Seismic interpretation of the Laga basin; Constraints on the structural setting and kinematics of the Central Apennines. *J. Geol. Soc. Lond.* **2011**, *168*, 179–190. [CrossRef]
51. Boschi, E.; Guidoboni, E.; Ferrari, G.; Valensise, G.; Gasperini, P. Catalogo dei forti terremoti in Italia dal 461 a.C. al 1990. *ING-SGA* **1997**, *2*, 644.
52. Stucchi, M.; Rovida, A.; Gomez Capera, A.A.; Alexandre, P.; Camelbeeck, T.; Demircioglu, M.B.; Gasperini, P.; Kouskouna, V.; Musson, R.M.; Radulian, M.; et al. The SHARE European Earthquake Catalogue (SHEEC) 1000-1899. *J. Seismol.* **2013**, *17*, 523–544. [CrossRef]
53. Blumetti, A.M. Neotectonic investigations and evidence of paleoseismicity in the epicentral area of the January-February 1703 Central Italy earthquakes. In *Perspectives in Paleoseismology*; Serva, L., Ed.; Bulletin of the American Association of Engineering Geologists: Boston, MA, USA, 1995; Volume 6, pp. 83–100.
54. Cello, G.; Mazzoli, S.; Tondi, E.; Turco, E. Active tectonics in the central Apennines and possible implications for seismic hazard analysis in peninsular Italy. *Tectonophysics* **1997**, *272*, 43–68. [CrossRef]
55. Cinti, F.R.; Cucci, L.; Marra, F.; Montone, P. The 1997 Umbria-Marche (Italy) earthquake sequence: Relationship between ground deformation and seismogenic structure. *Geophys. Res. Lett.* **1999**, *26*, 895–898. [CrossRef]
56. Cello, G.; Tondi, E. The Resolution of Geological Analysis and Models for Earthquake Faulting Studies. *J. Geodyn.* **2000**, *29*, 149. [CrossRef]
57. Galadini, F.; Galli, P. Active Tectonics in the Central Apennines (Italy)—Input Data for Seismic Hazard Assessment. *Nat. Hazards* **2000**, *22*, 225–268. [CrossRef]
58. Tondi, E.; Cello, G. Spatiotemporal evolution of the Central Apennines fault system (Italy). *J. Geodyn.* **2003**, *36*, 113–128. [CrossRef]
59. Roberts, G.P.; Michetti, A.M. Spatial and temporal variations in growth rates along active normal fault systems: An example from The Lazio–Abruzzo Apennines, central Italy. *J. Struct. Geol.* **2004**, *26*, 339–376. [CrossRef]
60. Mildon, Z.K.; Roberts, G.P.; Faure Walker, J.P.; Iezzi, F. Coulomb stress transfer and fault interaction over millennia on non-planar active normal faults: The Mw 6.5–5.0 seismic sequence of 2016–2017, central Italy. *Geophys. J. Int.* **2017**, *210*, 1206–1218. [CrossRef]
61. Chiaraluce, L.; di Stefano, R.; Tinti, E.; Scognamiglio, L.; Michele, M.; Casarotti, E.; Cattaneo, M.; de Gori, P.; Chiarabba, C.; Monachesi, G.; et al. The 2016 Central Italy Seismic Sequence: A First Look at the Mainshocks, Aftershocks, and Source Models. *Seismol. Res. Lett.* **2017**, *88*, 757–771. [CrossRef]
62. Pucci, S.; de Martini, P.M.; Civico, R.; Villani, F.; Nappi, R.; Ricci, T.; Azzaro, R.; Brunori, C.A.; Caciagli, M.; Cinti, F.R.; et al. Coseismic ruptures of the 24 August 2016, Mw 6.0 Amatrice earthquake (central Italy). *Geophys. Res. Lett.* **2017**, *44*, 2138–2147. [CrossRef]
63. Buttinelli, M.; Pezzo, G.; Valoroso, L.; de Gori, P.; Chiarabba, C. Tectonics Inversions, Fault Segmentation, and Triggerin Mechanisms in the Central Apennines Normal Fault System: Insights from High-Resolution Velocity Models. *Teconics* **2018**, *37*, 4135–4149. [CrossRef]
64. Civico, R.; Pucci, S.; Villani, F.; Pizzimenti, L.; de Martini, P.M.; Nappi, R.; The Open EMERGEO Working Group. Surface ruptures following the 30 October 2016 Mw 6.5 Norcia earthquake, central Italy. *J. Maps* **2018**, *14*, 151–160. [CrossRef]

65. Farabollini, P.; Angelini, S.; Fazzini, M.; Lugeri, F.R.; Scalella, G.; GeomorphoLab. La sequenza sismica dell'Italia centrale del 24 agosto e successive: Contributi alla conoscenza e la banca dati degli effetti di superficie. *Rend. Online Soc. Geol. Ital.* **2018**, *46*, 9–15. [CrossRef]
66. Villani, F.; Civico, R.; Pucci, S.; Pizzimenti, L.; Nappi, R.; de Martini, P.M.; The Open EMERGEO Working Group. A database of the coseismic effects following the 30 October 2016 Norcia earthquake in Central Italy. *Sci. Data* **2018**, *5*, 180049. [CrossRef]
67. Mazzoli, S.; Ascione, A.; Buscher, J.T.; Pignalosa, A.; Valente, E.; Zattin, M. Low-angle normal faulting and focused exhumation associated with late Pliocene change in tectonic style in the southern Apennines (Italy). *Tectonics* **2014**, *33*, 1802–1818. [CrossRef]
68. Mazzoli, S.; Santini, S.; Macchiavelli, C.; Ascione, A. Active tectonics of the outer northern Apennines: Adriatic vs. Po Plain seismicity and stress fields. *J. Geodyn.* **2015**, *84*, 62–76. [CrossRef]
69. Ryan, E.; Papeschi, S.; Viola, G.; Musumeci, G.; Mazzarini, F.; Torgersen, E.; Sørensen, B.E.; Ganerød, M. Syn-Orogenic Exhumation of High-P Units by Upward Extrusion in an Accretionary Wedge: Insights from the Eastern Elba Nappe Stack (Northern Apennines, Italy). *Tectonics* **2021**, *40*, e2020TC006348. [CrossRef]
70. Blender. Available online: https://www.blender.org/ (accessed on 24 August 2021).
71. Dovramadjiev, T. Principle of interaction between Worldwide Protein Data Bank and Blender software. In *Machines, Technologies, Materials, Proceedings of the XIII International Scientific Congress Winter Session, Borovets, Bulgaria, 16–19 March 2016*; Scientific-Technical Union of Mechanical Engineering: Sofia, Bulgaria, 2016; Volume 1, pp. 65–66.
72. Lanciani, M. Museo 3D: Ricostruzione e modellazione virtuale volta ad indagare il tema neogreco-neopompeiano durante l'esposizione internazionale a Roma del 1883. *Archeomatica* **2019**, *10*, 3.
73. Florinsky, I.V.; Filippov, S.V. Three-dimensional desktop morphometric models for the Artic Ocean floor. In Proceedings of the 29th International Cartographic Conference, Tokyo, Japan, 15–20 July 2019.
74. Basilici, M.; Mazzoli, S.; Megna, A.; Santini, S.; Tavani, S. 3-D Geothermal Model of the Lurestan Sector of the Zagros Thrust Belt, Iran. *Energies* **2020**, *13*, 2140. [CrossRef]
75. Basilici, M. Thermal Structure and Active Tectonics of the Frontal Zone of the Zagros Fold and Thrust Belt in Western Lurestan, Iran: New Insights from 3-D Geothermal Analytical Modelling and 2-D Structural Finite Element Modelling. Ph.D. Thesis, Università degli Studi di Urbino Carlo Bo, Urbino, Italy, 2021.
76. Dragoni, M.; Doglioni, C.; Mongelli, F.; Zito, G. Evaluation of Stresses in Two Geodynamically Different Areas: Stable Foreland and Extensional Backarc. *PAGEOPH* **1996**, *146*, 319–341. [CrossRef]
77. Springer, M. Interpretation of heat-flow density in the Central Andes. *Tectonophysics* **1999**, *306*, 377–395. [CrossRef]
78. Santini, S.; Basilici, M.; Invernizzi, C.; Mazzoli, S.; Megna, A.; Pierantoni, P.P.; Spina, V.; Teloni, S. Thermal Structure of the Northern Outer Albanides and Adjacent Adriatic Crustal Sector, and Implications for Geothermal Energy Systems. *Energies* **2020**, *13*, 6028. [CrossRef]
79. Cermak, V. Lithospheric thermal regimes in Europe. *Phys. Earth Planet. Inter.* **1993**, *79*, 179–193. [CrossRef]
80. Mele, G. Mapping the Moho across the Northern and Central Apennine chain and Eastern Sicily the teleseismic receiver functions method. In *The Earth Expansion Evidence—A Challenge for Geology, Geophysics and Astronomy, Proceedings of the 37th International School of Geophysics, Erice, Italy, 4–9 October 2011*; Scalera, G., Boschi, E., Cwojdzinski, S., Eds.; INGV: Rome, Italy, 2011.
81. Basilici, M.; Mazzoli, S.; Megna, A.; Santini, S.; Tavani, S. Geothermal Model of the Shallow Crustal Structure across the "Mountain Front Fault" in Western Lurestan, Zagros Thrust Belt, Iran. *Geosciences* **2019**, *9*, 301. [CrossRef]
82. Verdoja, M.; Chiozzi, P.; Gola, G. Unravelling the terrestrial heat flow of a young orogen: The example of the northern Apennines. *Geothermics* **2021**, *90*, 101993. [CrossRef]